JOURNAL OF MATERIALS SCIENCE 29 (1994) 189–202

Single-fibre polymer composites

Part I *Interfacial shear strength and stress distribution in the pull-out test*

ZONG-FU LI, D. T. GRUBB
Department of Materials Science and Engineering, Cornell University, Ithaca, NY 14853, USA

We have used Raman spectroscopy to measure the axial stress distribution along a fibre during a quasi-static single fibre pull-out test. The stress distribution at the debonding front during the progress of debonding gives the maximum interfacial shear strength τ_s directly. In addition, the stress distribution along the fibre after debonding can be used to evaluate the interfacial normal stress and the frictional coefficient. For the plasma treated high modulus polyethylene (PE) fibres used here, τ_s is found to be 28 MPa by this method, while the apparent mean interfacial shear strength τ_a obtained from the regular single fibre pull-out test varies from 3 to 15 MPa with the fibre embedded length l_e. Stress distributions derived from the shear-lag theory fit the experimental data for fully bonded fibres well, giving values for the shear-lag constant K and the stress transfer length $1/\beta$ [1]. According to the shear-lag theory, $\tau_s = \beta l_e \tau_a \coth(\beta l_e)$. If β can be found for a given system from Raman spectroscopy, τ_s can be evaluated from the pull-out test using this equation.

The regular pull-out tests, corrected for residual stress and interfacial friction, give the same τ_s but not the same β or pull-out load as the slower Raman test. The shear-lag constant K can be expressed as a function of the matrix shear modulus and geometric terms. One of these terms is the effective interfacial radius, r_e, the radius at which the strain in the matrix equals the average matrix strain. Raman measurements indicate that r_e is small, only four times the fibre radius. This result is supported by polarizing optical microscopy. The model of Greszczuk [2], which assumes a uniform shear within an effective interaction thickness b_i, gives a similar result. We find that $b_i = 20$ μm, about twice the fibre radius. Using the pull-out test data, as for other fibre composites, b_i and r_e predicted by shear-lag theories do not agree with the results of microscopy to this extent. In these cases τ_s is much larger than the yield strength of the matrix and as neither treatment considers plastic deformation of the matrix agreement should not be expected.

1. Introduction

The interface between the fibre and matrix in fibre reinforced composites plays a very important role in determining composite mechanical properties. The goal of many composite studies is to tailor the interfacial properties to achieve the best composite properties. A strong interface improves the compressive strength and transverse tensile strength of the composite, but may be detrimental to tensile and fracture strength. This is because a matrix failure mode may become dominant [3]. Generally, fibre reinforced polymeric resin composites should have a good interfacial shear strength (IFSS) to be acceptable products. To achieve the desired interface properties, fibre surface coatings and surface treatments are often adopted. Better understanding of the interface has led to more sophisticated practices of control and design. Examples are incorporation of an interphase having a modulus between that of fibre and matrix, and having a modulus gradient in the interface [4, 5]

One key property is the interfacial shear strength (τ_s), which depends on the fibre surface properties and the mechanical properties of the fibres and the matrix. The test methods most often used for determining τ_s are the fibre fragmentation test, the fibre push-down or indentation method, and the single fibre pull-out test. High modulus polymer fibres fibrillate on fracture. This makes it difficult to determine the exact fragmentation length in the fibre fragmentation test [6]. Indentation of the polymer fibre ends can also cause fibrillation instead of interfacial debonding. This leaves the single fibre pull-out test, which does not cause fibrillation, as the method of choice for determining τ_s of high modulus polymer fibres. In the test a length of fibre l_e is embedded in a matrix and pulled out, and the maximum stress σ_p causing complete interfacial debonding is measured. It is normally assumed that the shear stress along the whole of the interface can be approximated as a constant, τ_a. Then from a simple force balance:

$$\tau_a = \sigma_p r_f / 2 l_e \quad (1)$$

where r_f is the fibre radius. The value of τ_a is often used as τ_s, although it varies with the test geometry, and is

0022–2461

a strong function of the fibre embedded length l_e. This "determination" of interfacial shear strength ignores stress concentrations, and τ_a is better described as the apparent mean interfacial shear strength. Before interfacial debonding, the shear stress at the interface has a maximum where the fibre enters the matrix, and if l_e is long, the shear stress at the interface falls to zero within the composite. This is well known, and it means that pull-out tests with short embedded lengths will give a more realistic value of τ_s.

To improve pull-out testing, very short embedded lengths may be used, and various models can also be used to obtain the true IFSS from τ_a. These are well summarized by Désarmot and Favre [9]. Using a shear stress criterion for interfacial failure, the maximum shear stress τ_{max} at debonding is the true τ_s and must be independent of l_e. According to shear-lag theory, τ_s is related to the apparent interfacial shear strength as:

$$\tau_a = \tau_s \frac{\tanh(\beta l_e)}{\beta l_e} \quad (2)$$

This equation is derived and β is defined later in the paper. From this relation, τ_s corresponds to τ_a at $l_e = 0$ and it can be obtained from τ_a at any l_e when β is known. One way to obtain β is to fit the experimental values of τ_a versus l_e to Equation 2. Results for τ_a at small l_e and a large set of data are required for an accurate determination of β and thus τ_s. If l_e is large, so that $\beta l_e > 5$, then $\tanh(\beta l_e) \approx 1$ and

$$\tau_a \approx \tau_s/(\beta l_e) = C/l_e \quad (3)$$

Pitkethly and Doble [7] use this approximation in a two stage fitting procedure, with data at large l_e giving a value for C. Rewriting Equation 2 as:

$$\tau_s(l_e/C) = \operatorname{arctanh}(\tau_a l_e/C) \quad (4)$$

the slope of a plot of $\operatorname{arctanh}(\tau_a l_e/C)$ versus l_e/C gives τ_s. Even using this method, data at small embedded lengths are required for an accurate determination of the interfacial shear stress.

Test specimens with small l_e are difficult to produce. One method is to place a small drop of resin on a single free fibre and cure it [8]. Difficulties with this method are that the exact size of the drop is not easily reproducible and the classic shear-lag theory may not be applicable because of the complexity of the stress field in the small drop. Other methods involve dipping the fibre into liquid epoxy resin to a small controlled depth [9, 10]. In this case, the contact meniscus at the fibre entrance into the matrix is a problem in defining l_e and the bonding stress at the fibre end will contribute to the fibre pull-out stress. The values of τ_s obtained by these methods at small l_e are often much larger than the yield shear strength of the matrix. Plastic deformation should then occur at the interface and the classic shear-lag theory no longer applies. The determination of τ_s then lacks self-consistency and may not represent the true interfacial shear strength [10].

In this study we will show that the axial stress distribution along the embedded length obtained by Raman spectroscopy can be used to calculate β and thus τ_s. Raman spectroscopy has been used to measure the axial fibre stress or strain in a range of high modulus fibres [11–14] and the molecular stress distribution within fibres [15–18]. The principle is that when a tensile stress is applied to a high modulus fibre, bonds in the backbone of molecules stretch and bond angles increase. This makes the frequencies of Raman active modes decrease. The most significant frequency shifts arise from the stretching of bonds such as the aromatic and heterocyclic ring in aramids [11, 12], the C≡C bonds in poly(diacetylene) [13], and the C–C bonds in the graphite basal plane of carbon fibres [14]. In these cases the vibrational frequency shift is linear with stress all the way to fibre failure. Recently, the Raman spectroscopy of high modulus polyethylene (PE) fibres has been studied by Prasad and others [15–17]. They found that the C–C asymmetric stretch band shifts the most with stress, but at room temperature it shifts linearly only up to 0.5 or 1 GPa, depending on the fibre type. Above this stress, plastic deformation occurs and the band shape changes.

Raman spectroscopy has also been applied to measure the axial stress (or strain) distribution along fibres in composites, and to follow the micromechanics of load transfer from fibre to matrix. Galiotis *et al.* [19] used a model composite system containing one short poly(diacetylene) single crystal fibre in an epoxy resin matrix. They found that when the composite was loaded in tension the stress distribution along the fibre agreed well with shear-lag theory predictions [1]. (Some unknown parameters were allowed to vary, so only qualitative agreement was demonstrated). Fan *et al.* [20] used Raman spectroscopy to find that a thin coating of a silicone release agent does not affect the stress distribution. Jahankhani and Galiotis [21, 22] investigated the stress transfer in a Kevlar fibre/epoxy composite both in tension and in compression. The load transfer length at interfacial failure and the interfacial shear strength were obtained by loading the composite to the strain at which interfacial debonding occurred. By compressing the model composite system, the compressive strain at which the fibre buckles within the matrix can be determined. A method based on this measurement has been proposed for measuring the compressive strength of Kevlar and carbon fibres [21, 23]. Although the technique is limited to near-surface fibres or transparent matrices, Raman spectroscopy provides a unique *in situ* measurement of fibre stress in composites.

Recently, Grubb and Li [24] have reported preliminary results obtained by applying the Raman technique to the single fibre pull-out test. The axial stress distribution in high modulus PE fibres and a value for the τ_s were obtained. Meanwhile, Boogh *et al.* [25] studied the stress distribution in a high modulus PE fibre embedded in epoxy tensioned to a fixed strain. The efficiency of the load transfer was determined in terms of the load transfer length for different surface treatments and curing conditions. They showed that curing at a high temperature caused an increase in the stress transfer length or a decrease of interfacial shear

strength. Their data did not demonstrate the existence of compressive residual stress in the fibres due to matrix shrinkage. We have investigated the residual stresses in fibres caused by curing shrinkage of the matrix and mismatch of the thermal coefficient of expansion. The effects of these stresses on the composite interface and stress transfer are reported in the second of this series of papers [26].

High modulus PE fibres are used in our model composites to investigate the interfacial shear strength using Raman spectroscopy. The fibres are easy to handle and are not damaged by absorption of the laser light. They also have a very high tensile strength, a small compressive strength and a very small thermal coefficient of expansion in the fibre direction. More important is a Raman spectrum free of fluorescence, and a comparatively weak interface to the epoxy matrix. This allows them to be pulled out of the composites from a large embedded depth l without significant plastic deformation at the interface. Other fibres, such as aramids, break when pulled from embedded lengths over 0.25 mm [8]. Untreated PE fibre composites have a too weak interface; the fibres used here are plasma treated. One extraordinary property of the PE fibres is their large positive thermal coefficient of expansion (TCE) in the radial direction. It is approximately $13 \times 10^{-5}\,°C^{-1}$ [27], while that of the epoxy matrix is $6 \times 10^{-5}\,°C^{-1}$. This will cause radial tensile stress at the interface on cooling from the curing temperature.

2. Analytical aspects of single fibre pull-out test

Among the many theoretical analyses of load transfer during fibre pull-out, [2, 28–38], the shear-lag analysis based on the assumption of pure shear first proposed by Cox [1] gives the simplest analytical solution [2, 28–31]. Gray [39] reviewed a number of early works on shear-lag analysis. Several authors have shown that the stress distribution predicted by shear-lag theory agrees reasonably well with experimental distributions [20, 22, 40]. Aksel *et al.* [41] compared the stress distributions obtained using finite element analysis with shear-lag analysis for a partially debonded interface. They showed that shear-lag analysis accurately predicts the fibre axial stress and the interfacial shear stress when the frictional coefficients are small and the debonded length is much larger than the fibre diameter. Elaborate analyses using elasticity for the exact stress field have been performed by Muki *et al.* and Ford [32, 33]. Exact solutions are obtained only when the fibre and matrix are taken to be isotropic. Ford's solution differs from Muki's in the treatment of the stress singularity at the interface where the fibre enters the matrix. McCartney [34] smoothed the stress singularity by averaging the stresses over the fibre and the matrix. He obtained approximate analytical solutions of the stress distributions for a fully bonded and for a partially debonded interface. Steif and Hoysan [35] analysed the load transfer for an imperfectly bonded interface by formulating the relative displacement at the interface into an edge dislocation problem and relating the interfacial shear stress to the dislocation density. They obtained an analytical solution only in the case when the fibre and matrix have the same elastic properties. Sigl *et al.* [36, 37, 38] analysed the interfacial debonding process and fibre pull-out over interfacial friction and the energetics of the propagation of interfacial debonding. Aveston *et al.* [29, 30, 31] used the fibre axial stress and interfacial shear stress obtained from shear-lag analysis to derive the strain energy involved in steady state interfacial debonding. In the following we use the shear-lag theory to derive the stress distribution along the single fibre in an infinite matrix giving particular consideration to the fibre residual stress and to partial debonding of the fibre.

The fibre pull-out configuration when the fibre has a fully bonded interface is shown in Fig. 1(a), where x is the position along the fibre axis of the embedded fibre of radius r_f. The fibre has an axial stress function $\sigma_f(x)$ and so the external stress applied to the fibre is $\sigma_0 = \sigma_f(0)$, assuming that the stress at the fibre cross-section is uniform. To keep the matrix surface at $x = 0$ and the tensile stress positive when acting towards $+x$, the embedded fibre lies from $-l$ to 0 and so all values of x in the useful ranges of the following formulae are negative. Consider $\tau_i(x)$ to be the interfacial shear stress along the fibre, $u_f(x)$ the axial fibre displacement, and $u_m(x, r)$ the displacement of matrix in the x direction as a function of radial distance r out from the fibre axis at x. The assumptions of the shear-lag theory are:

(i) at the bonded interface $u_f(x) - u_m(x, r_f) = 0$, i.e. there is no slippage between fibre and matrix at the interface—perfect bonding;
(ii) at the debonded interface $u_f(x) - u_m(x, r_f) > 0$, here the shear stress is taken by interfacial friction.

The matrix curing shrinkage is treated as if it were due to hydraulic pressure acting on all sides of the matrix and not the fibre. When no external load is applied to the fibre, the fibre is free of stress at both ends, but has a residual strain equal to the matrix curing shrinkage at positions sufficiently far away from both the ends.

Following Cox [1] in assuming that the stress state of the matrix is pure shear, the equilibrium equation

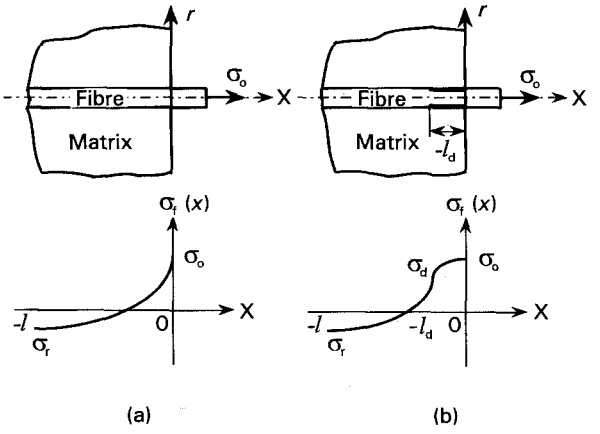

Figure 1 Schematics of single fibre pull-out. (a) Fibre axial stress distribution for a fully bonded interface. (b) Fibre axial stress distribution for a partially debonded interface.

for the shear stress in the matrix simplifies to

$$\frac{\partial \tau_m(x, r)}{\partial r} + \frac{\tau_m(x, r)}{r} = 0 \quad (5)$$

The matrix shear stress can also be expressed in terms of the displacements $u_m(x, r)$ and the shear modulus G_m of the matrix:

$$\tau_m(x, r) = G_m \frac{\partial u_m(x, r)}{\partial r} \quad (6)$$

The above relations have the solutions of

$$\tau_m(x, r) = \tau_i(x) r_f / r \quad (7)$$

$$\tau_i(x) = \{u_f(x) - u_r(x)\} \frac{G_m}{r_f \ln(r_e/r_f)} \quad (8)$$

where $u_r(x)$ is the matrix displacement along the x direction due to matrix curing shrinkage, and r_e is the radius of matrix at which the strain in the matrix equals the average matrix strain, so $u_m(x, r_e) = u_r(x)$ at r_e.

For a single fibre in a finite specimen r_e should be the radius or some other dimension of the specimen. For an infinite matrix, according to Equation 5, $\tau_m(x)$ becomes zero only when $r \to \infty$, and this leads to a logarithmic divergence of the right hand side of Equation 8, and in the shear-lag constant K, defined below in Equation 13. Many experimentalists have tried to calculate the stress distribution using the specimen dimension as r_e for a single fibre composite specimen [20, 22, 42]. In the original work of Cox, the fibre volume fraction is large and r_e is taken as the mean separation of fibres [1]. For fibres closely packed into an hexagonal array, $r_e/r_f = 2$, $u_m(x, 2r_f) = u_r(x)$, according to Equation 8. This means the matrix shear stress at $r = 2r_f$ is negligible. But according to Equation 7, the matrix shear is $\tau_i(x) r_f / r_e$ equal to one half the interface shear stress, $\tau_i(x)$. The effect of this half the $\tau_i(x)$ on local displacement is not negligible.

Clearly Cox oversimplified the matrix stress field by assuming pure shear stress in the matrix. In reality, the shear stress in the matrix drops quickly. It reaches zero a few fibre diameters away from the fibre, and this can be observed directly by optical microscopy of the stress birefringence. Our later determination of K also shows that r_e/r_f is small (≈ 4), even for a sample containing a single fibre. Budiansky *et al.* [31, 41] assumed that a matrix cylinder with outer radius r_e can be abstracted from the infinite matrix and concentrated all of the axial stress-carrying area at r_e while assuming the matrix in the region supports pure shear stress $\tau_m(x, r)$. If r_e/r_f is sufficiently large, say over 5, then the effect of the fraction of $\tau_i(x)$ on matrix displacement beyond r_e can be negligible. Greszczuk [2] assumes that there is an effective width to the interface, b_i, beyond which the fibre has no influence on the matrix, and that the shear stress is constant within this region. The shear-lag constant expression then becomes

$$\tau_m(x, z) = \tau_i(x) = G_m \frac{\partial U(x, z)}{\partial z} = G_m \Delta u(x) b_i \quad (9)$$

$$K = \frac{G_m}{b_i} \quad (10)$$

The classic shear-lag analysis first proposed by Cox assumed the interfacial shear stress

$$\tau_i(x) = K\{u_f(x) - u_m(x)\} = K\Delta u(x), \quad (11)$$

where $u_m(x)$ is the mean matrix displacement that would be present if the fibre was replaced by matrix. A simplification can be made by treating the load as uniformly distributed on the cross-section of the matrix, so that

$$u_m(x) = (\varepsilon_a + \varepsilon_r)x = \frac{\sigma_0}{E_m} \frac{A_f}{A_f + A_m} x + \varepsilon_r x \quad (12)$$

where ε_a is the strain due to the external load, A_f and A_m are the cross-sectional areas of the fibre and matrix, respectively, and ε_r is the matrix curing shrinkage. For a single fibre pull-out specimen, $A_f \ll A_m$, so ε_a is negligibly small, and $u_m(x)$ is simply identical to $u_r(x)$. Then

$$K = \frac{G_m}{r_f \ln(r_e/r_f)}. \quad (13)$$

A force balance at the interface gives the relationship between the longitudinal stress on the fibre $\sigma_f(x)$ and the interfacial shear stress $\tau_i(x)$ as

$$\frac{d\sigma_f(x)}{dx} = \frac{2\tau_i(x)}{r_f} \quad (14)$$

Substituting for $\tau_i(x)$ from Equation 8 and differentiating to go from displacements $u(x)$ to strains $\varepsilon(x)$ we obtain:

$$\frac{d^2\sigma_f(x)}{dx^2} = \frac{2K}{r_f}\{\varepsilon_f(x) - \varepsilon_m(x)\} = \frac{2K}{E_f r_f}\{\sigma_f(x) - \varepsilon_r E_f\} \quad (15)$$

where E_f is the axial fibre modulus and ε_r is the matrix shrinkage strain, a constant. This equation has solutions of the form:

$$\sigma_f(x) = E_f\varepsilon_r + A\cosh(\beta x) + B\sinh(\beta x) \quad (16)$$

A and B are coefficients to be determined by the boundary conditions, and

$$\beta = \sqrt{\frac{2K}{E_f r_f}} \quad (17)$$

If the deformations are elastic, then $E_f\varepsilon_r$ is simply equal to the axial residual stress (σ_r) of the fibre. When the fibre is perfectly bonded to the matrix along its entire length, one boundary condition is $\sigma_f(0) = \sigma_0$. Another boundary condition satisfies the global axial load balance in the specimen at $x = -l$:

$$\sigma_f(-l)A_f + \sigma_m(-l)A_m = \sigma_0 A_f + E_m\varepsilon_r A_m \quad (18)$$

Because $A_m \gg A_f$, the additional stress in fibre and matrix due to applied load is negligible, and $\sigma_f(-l) = \sigma_r$. Then

$$\sigma_f(x) = \sigma_r + (\sigma_0 - \sigma_r)\{\cosh(\beta x) + \coth(\beta l)\sinh(\beta x)\} \quad -l \le x \le 0 \quad (19)$$

$$\tau_i(x) = \frac{r_f\beta}{2}(\sigma_0 - \sigma_r)\{\sinh(\beta x) + \coth(\beta l)\cosh(\beta x)\}$$
$$-l \le x \le 0 \quad (20)$$

$$\tau_{max} = \tau_i(0) = \frac{r_f\beta}{2}(\sigma_0 - \sigma_r)\coth(\beta l) \quad (21)$$

$$\tau_{ave} = \frac{(\sigma_0 - \sigma_r)r_f}{2l} = \frac{1}{l}\int_{-l}^{0}\tau_i(x)\,dx = \tau_{max}\frac{\tanh(\beta l)}{\beta l} \quad (22)$$

Here τ_{max} and τ_{ave} refer to the maximum and average interfacial shear stresses at any given external load. When debonding begins, Equation 22 becomes the same as Equation 2; $\tau_{max} = \tau_s$, but τ_{ave} differs slightly from τ_a given in Equation 1 because the residual stress σ_r is ignored in Equation 1.

For long fibre embedded lengths, where the axial stress in the fibre falls to the residual stress well before the end of the fibre, $l \ge 5/\beta$, $\coth(\beta l) \approx 1$, and the above equations simplify to:

$$\sigma_f(x) = \sigma_r + (\sigma_0 - \sigma_r)e^{\beta x} \quad -l \le x \le 0 \quad (23)$$

$$\tau_i(x) = \frac{r_f\beta}{2}(\sigma_0 - \sigma_r)e^{\beta x} \quad -l \le x \le 0 \quad (24)$$

$$\tau_{max} = \frac{r_f\beta}{2}(\sigma_0 - \sigma_r) \quad (25)$$

$$\tau_{ave} = \frac{r_f}{2l}(\sigma_0 - \sigma_r) = \frac{\tau_{max}}{\beta l} \quad (26)$$

Now let us consider the case of a partially debonded interface, as illustrated in Fig. 1(b). The debonded part extends from $x = 0$ to $x = -l_d$. For the bonded part of interface from $-l_d$ to $-l$, Equation 14 still holds and its solution has the same form as Equation 16. One boundary condition is still that $\sigma_f(-l) = \sigma_r$, and the other is based on the assumption that the interfacial shear strength τ_s is a material constant. Then interfacial debonding occurs when the maximum interfacial stress reaches this value, and it occurs at $x = -l_d$. The shear stress at the point of debonding will be infinite if the crack tip is sharp [33]. However, plastic deformation at the tip will reduce the stress at the tip to a finite value.

$$\tau_i(-l_d) = \frac{r_f}{2}(d\sigma_f/dx)_{x=-l_d} = \tau_s \quad (27)$$

The upper limit of τ_s is the matrix yield strength. The results for the coefficients A and B, and for the fibre axial stress in the bonded region are:

$$A = \frac{2\tau_s}{\beta r_f\{\coth(\beta l)\cosh(\beta l) - \sinh(\beta l)\}} \quad (28)$$

$$B = A\coth(\beta l) \quad (29)$$

$$\sigma_f(x) = \frac{2\tau_s}{\beta r_f}\left\{\frac{\tanh(\beta l)\cosh(\beta x) + \sinh(\beta x)}{\cosh(\beta l_d) - \tanh(\beta l)\sinh(\beta l_d)}\right\} + \sigma_r \quad -l \le x \le -l_d \quad (30)$$

Again, for long fibre embedded lengths the axial stress in the fibre falls to the residual stress well before the end of the fibre. That is, for $l \ge 5/\beta$, $\coth(\beta l) \approx 1$ and the expression for fibre stress then simplifies to:

$$\sigma_f(x) = \sigma_r + \frac{2\tau_s}{\beta r_f}\exp[\beta(x + l_d)] \quad -l \le x \le -l_d \quad (31)$$

$$\sigma_d = \sigma_f(-l_d) = \sigma_r + 2\tau_s/\beta r_f \quad (32)$$

Note that $\sigma_f(-l_d)$ is independent of l and l_d, if l is large.

Along the debonded part of the interface, the fibre is being pulled out against friction. $\sigma_f(x)$ depends on the frictional coefficient, f, and normal stress, $N(x)$, if $N(x)$ is compression. Assuming Coulomb friction, a simple force balance if deformations remain elastic, and that the fibre is still in contact with the matrix gives:

$$\frac{d\sigma_f(x)}{dx} = \frac{2}{r_f}fN(x) \quad (33)$$

$N(x)$ is proportional to the fibre normal strain, $\varepsilon_i(x)$, caused by the misfit between fibre and matrix. Following Timoshenko [44], $N(x)$ in a shrink fit configuration with no external load applied to the fibre is given by

$$N(x) = \frac{\varepsilon_i(x)}{(1 + \nu_m)/E_m + (1 - \nu_f)/E_f} \quad (34)$$

where ν_f and ν_m are the Poisson's ratios of fibre and matrix, respectively. Pinchin and Tabor [45] applied this relation to the case when an external load is applied to the fibre. They split $\varepsilon_i(x)$ into two components: ε_0 which is the misfit strain when no external load is applied and $\varepsilon_1(x)$ which is due to the lateral contraction of the fibre as it is stretched axially. ε_0 is due to differential thermal contraction, matrix curing shrinkage or the misfit of an irregular diameter fibre [26]. $\varepsilon_1(x)$ will be linear with the local longitudinal strain σ_f/E_f.

$$\varepsilon_i = \varepsilon_0 - \nu_f\sigma_f(x)/E_f \quad (35)$$

$$N(x) = N_0 - \xi\nu_f\sigma_f(x) \quad (36)$$

where

$$\xi = 1\Big/E_f\left(\frac{1 + \nu_m}{E_m} + \frac{1 - \nu_f}{E_f}\right)^{-1} \quad \text{and} \quad N_0 = \xi\varepsilon_0$$

Tsai and Muri [38] analysed the exact stress field in the debonded region in more detail for a finite volume fraction of fibres. When the volume fraction is set equal to zero, their expressions for ξ and $N(x)$ are exactly the same as above. Substituting this expression for $N(x)$ into Equation 33 and setting $\sigma_f(-l_d) = \sigma_d$, which is defined in Equation 32,

$$\sigma_f(x) = \gamma + (\sigma_d - \gamma)\exp[-\alpha(l_d + x)] \quad -l_d \le x \le 0 \quad (37)$$

where $\gamma = N_0/(\nu_f\xi)$, $\alpha = 2f\nu_f\xi/r_f$. The applied tensile stress becomes

$$\sigma_0 = \gamma + (\sigma_d - \gamma)\exp(-\alpha l_d) \quad (38)$$

This relates debonding length l_d to the external fibre stress.

When debonding is complete, friction is established over the whole fibre. Before the fibre slips, the external load is carried over an embedded length l_{eff}, called the

effective frictional stress transfer length, where $\sigma_f(-l_{eff}) = 0$. Then

$$\sigma_f(x) = \gamma\{1 - \exp[-\alpha(l_{eff} + x)]\} \quad -l_{eff} \leq x \leq 0 \tag{39}$$

When l_{eff} approaches the total embedded length l_e, the fibre begins to slip out, $l_{eff} = l_e$, and the external load decreases as l_e falls.

$$\sigma_0 = \gamma[1 - \exp(-\alpha l_e)] \tag{40}$$

We will show in Part 2 of this paper that α and γ can be determined by curve fitting the experimental stress distributions obtained by Raman spectroscopy [26]. Once α and γ are known, N_0 and f can be calculated.

There are two criteria applied to the initiation of interfacial debonding [9, 10]. One is the maximum interfacial strength criterion, which states that the interface debonding initiates when τ_{max} approaches τ_s. This has been used by Aksel *et al.* [41] to derive the debonded length and in the above analysis, for example in deriving the boundary conditions for a partially debonded fibre. According to this criterion, τ_s is a material constant. With this criterion and neglecting effects at the end of the embedded fibre, we can take $l = l_e$, then the pull-out stress σ_p will be

$$\sigma_p = \frac{2\tau_s}{r_f\beta}\tanh(\beta l_e) + \sigma_r \tag{41}$$

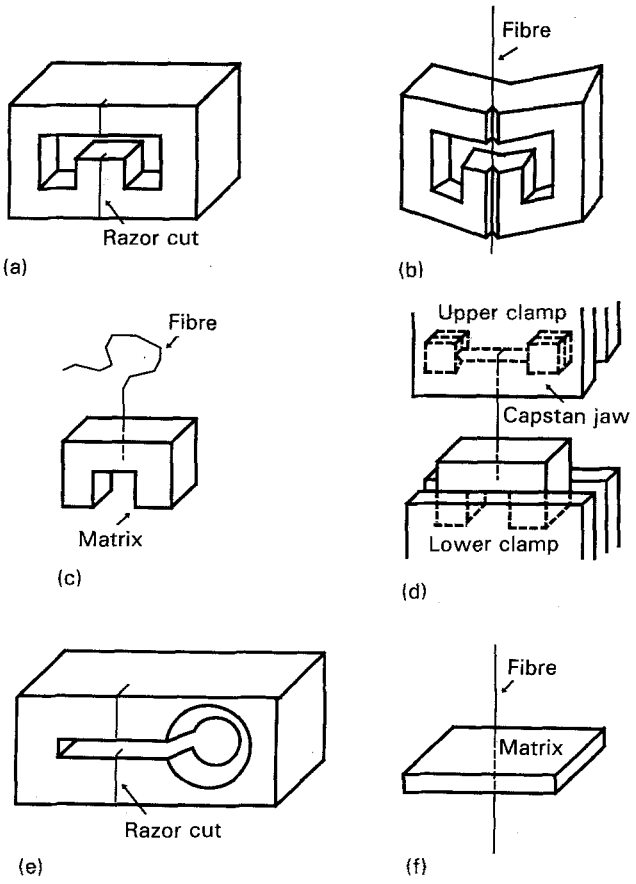

Figure 2 Schematic of single fibre pull-out specimen preparation and pull-out test. (a) Silicone rubber mould, (b) placing a fibre into mould, (c) moulded single fibre pull-out specimen, (d) single fibre pull-out test, (e) silicone rubber mould for pull-out specimen of small embedded fibre length, (f) fibre pull-out from a thin sheet of matrix.

when friction can be neglected (true if the embedded length l_e is small). Using Equation 30 it is found that σ_d is constant until all but the last part of the fibre, length approximately $1/\beta$, is reached. Friction is important for long l_e, $\beta l_e \gg 1$; in this case, the last part of the fibre where σ_d drops can be neglected. The σ_d in Equation 37 can be replaced with σ_p at $\beta l_e \gg 1$, $2\tau_s/\beta r_f$ and $l_d \approx l_e$ at the maximum value of σ_0. The peak pull-out stress when friction cannot be neglected is then

$$\sigma_p = \gamma + \left(\frac{2\tau_s}{r_f\beta} + \sigma_r - \gamma\right)\exp(-\alpha l_e) \tag{42}$$

The other criterion for the initiation of interfacial fracture is the interfacial fracture energy criterion. This states that interfacial debonding initiates when the strain energy in the fibre pull-out system approaches the interfacial fracture energy, G_i. It has been discussed by several authors [36–38]. Piggot has argued that the energy criterion is appropriate because the interfacial shear stress was found to exceed the matrix yield strength for many composites [46]. Based on Piggot's expression for zero free fibre length, Désarmot and Favre [9] obtained the following expression for the debonding stress with the free fibre length of L_f:

$$\sigma_p = 2\sqrt{\frac{\beta G_i E_f l_e/r_f}{\coth(\beta l_e) + \beta L_f}} \tag{43}$$

They found that their experimental data did not fit this equation and therefore chose the stress criterion for debonding [9]. We find that this expression can fit our experimental data fairly well, but the fit gives standard deviations for β and G_i a few times larger than those for β and τ_s using the stress criterion. In the rest of this paper we will use the stress criterion.

3. Experimental procedures

3.1. Materials and specimen preparation

The fibres in these fibre composites were commercial high modulus polyethylene materials, Spectra 900 and Spectra 1000, produced by Allied Signal. The fibres were treated with an ammonia plasma for improved adhesion [47]. DGEBA-type epoxy resin, DER 331, and tetraethylene pentamine curing agent, DEH 26, were obtained from Dow Chemical Company. They were mixed stoichiometrically according to the manufacturer's specifications.

The single fibre pull-out specimens were prepared using a silicon rubber mould based on the mould technique developed by Li and Netravali [48]. Fig. 2 illustrates the procedure schematically. First, a metal die is made in the required shape for the epoxy, and a silicone rubber mould is cast around the die. After the rubber mould is cured and the die is removed, a razor cut is made in the mould where the fibre is to go. The cut is made to exactly half the depth of the die cavity. Fig. 2(a). Then the mould is flexed to open the cut into a V-shaped crack and a fibre under slight tension (from a small weight) is placed straight in the cut, as shown in Fig. 2(b). The mould is then released to grip the fibre. The mixture of epoxy resin and curing agent is then cast and cured in the mould

around the fibre. The epoxy curing time is 4 h at a curing temperature of 100 °C and at least overnight at room temperature. After curing, the epoxy can be separated easily from the mould and removed by bending the mould slightly. The lower part of the fibre is trimmed using a razor blade, and the specimen, as shown in Fig. 2(c), is ready for the fibre pull-out test.

Specimens used for Raman spectroscopy or for photoelastic observation must have flat polished surfaces to reduce light scattering and allow accurate focusing. Time consuming metallographic polishing of each specimen is often required, but here only the original metal die is polished. The surface of the molded epoxy resin made this way is smooth so that no further polishing is necessary. Another important advantage of the moulding technique for the single fibre pull-out test is that there is no contact meniscus where the fibre enters the epoxy. In other sample preparation methods currently used for this test, a fibre is inserted into the free surface of the epoxy [9, 10] and the surface does not remain flat. A flat surface is particularly important when the embedded length l_e is small. For displacement controlled pull-out tests with small l_e, the fibre is embedded in two pieces of epoxy with different embedded lengths. The piece with longer l_e acts as a tabbed grip for the fibre and pull-out is suppressed by the clamping forces. The free fibre length is the separation of the two cavities, 10 mm in these tests.

These modifications to the original moulding technique [48] work for embedded lengths down to 0.5 mm. Further developments allow the preparation of specimens with l_e at least as small as 0.2 mm. A thin metal sheet is used as the die to define the cavity in the silicone rubber mould. The thickness of the sheet defines the cavity width and thus the fibre embedded length. After the mould is made, a small reservoir where a drop of liquid epoxy is to be deposited is cut at one edge of the cavity, as shown in Fig. 2(e). The mould is sprayed with a mould release agent so that the cured epoxy can be removed from the mould easily. The mould is then heated to remove residual solvent from the release agent. This would cause bubbles in the epoxy during curing. The epoxy drop is then deposited in the reservoir and easily fills the narrow cavity. The result is a thin sheet of epoxy with the fibre passing through the middle of the sheet. This geometry begins to approach that of the micro-bond test [8], where the fibre is pulled through a drop of epoxy, but in this method the sample geometry and the loading geometry are under good control. The lower part of fibre is not trimmed in this specimen because trimming may cause debonding of a significant part of the interface when l_e is small.

The micro-bond and other such tests must have a distribution of bead sizes and embedded lengths. The mean value of τ_a from these tests has a large coefficient of variation, over 20% [49], and there have been a number of serious questions regarding interpretation of the derived τ_a and the limitations of this method [50]. The embedded length in the method described here is under precise control and a number of specimens of the same embedded length can be prepared to obtain a mean value of τ_a for a given embedded length. The coefficient of variation is found to be less than 20% when only ten specimens were tested for each embedded length. These results will be shown in Fig. 6. The main problem with this method is that it is difficult to remove the sample for the mould without bending or damaging the fibre. This currently limits the application to more flexible fibres, such as high modulus polyethylene and aramid fibres.

3.2. Fibre pull-out tests

A small loading frame designed to fit on the microscope stage of the Raman equipment and capable of loading samples by dead weights or controlled strains was used for single fibre pull-out during Raman and photoelastic observation. Regular single fibre pull-out tests were carried out on an Instron tensile machine, model 1122. Fig. 2(d) shows a schematic of these fibre pull-out tests for specimens with $l_e \geq 1$ mm. The fibre is embedded in a bridge-shaped piece of epoxy which is easily gripped by a clamp without stressing the test region. The other end of the fibre is gripped by a capstan jaw [51] which is clamped in the moving cross-head of the Instron. Fig. 2(f) illustrates the fibre pull-out test for specimens with $l_e < 1$ mm. The thin sheet of epoxy is placed under a microvice. The fibre is pulled up through a gap of 0.5 mm between the two plates of the microvice at a strain rate of 0.02 min^{-1}. For all these tests, 10 specimens were tested to obtain a mean value of τ_a for each embedded length and fibre surface and epoxy curing condition. The diameter for each fibre was obtained using a vibroscope following ASTM D1577-79. Raman spectra were taken at different positions along the embedded fibre while it was held under load using a dead weight or held at a fixed strain. For fixed strain tests the fibre was embedded at both ends, with a free fibre length of 10 mm. Significant stress relaxation takes place when the fibre is tensioned at a fixed strain. Samples were tensioned several times to approximately the same stress value until no significant stress drop occurred (Fig. 3). A stable debonding length is achieved after a few cycles of reloading. The loading process is called the quasi-static process. When a specimen is loaded by a dead weight, creep occurs at the interface, causing interfacial debonding at a lower external load than that obtained from the regular test. Debonding is stabilized within a few hours, or continues to completion.

It has previously been shown that the Raman 1063 cm^{-1} peak frequency shifts at -5 ± 0.5 cm^{-1} GPa^{-1}, proportional to the axial fibre stress up to tensile stresses of 0.5 GPa for Spectra 900 fibres and 1 GPa for Spectra 1000 fibres [15, 17]. It is important to keep the maximum fibre stress during loading below 0.5 GPa or 1 GPa for Spectra 900 and Spectra 1000, respectively, if Raman shift is to be used as a stress gauge.

3.3. Raman spectroscopy

Raman spectra were obtained using a SPEX 1877 Triplemate spectrometer, equipped with a holo-

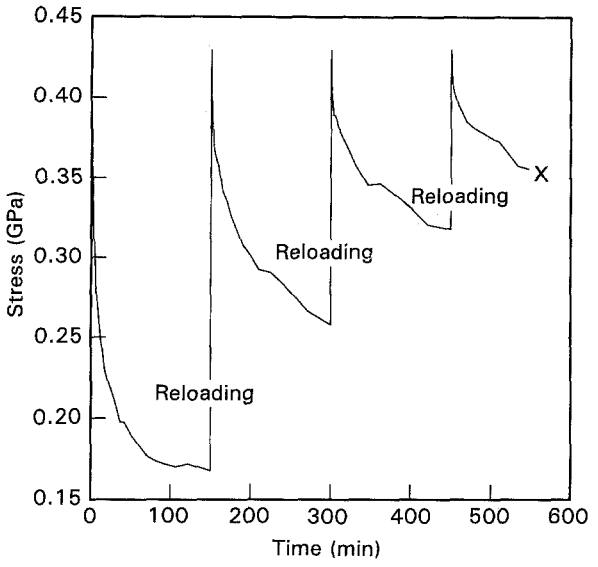

Figure 3 Stress of fibre as a function of time during stress relaxation and reloading.

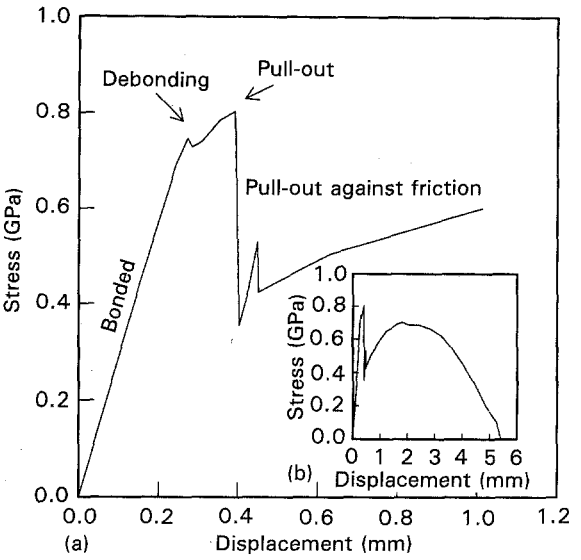

Figure 4 Stress versus displacement of a single fibre pull-out. The main plot shows the first 1 mm of displacement, and the inset is the whole curve.

graphic grating of 1800 grooves mm^{-1} at the spectrograph stage. The source is a 2W Ar^+ laser (Coherent Nova 90-5) operating at 514.5 nm. The laser is focused on the specimen using a Leitz microscope with a 10× objective to a spot $\approx 10\ \mu m$ in diameter. The power of the laser beam at the specimen is about 25 mW. The detection system is a diode array covering 400 cm^{-1}, an EG&G optical multi-channel analyzer. The spectra are calibrated using a neon or argon light source. The wavenumber shift of the peak of the C–C asymmetric stretch band is used to measure the tensile or compressive axial stress in the fibres. Measured values of the peak position of this band in free unstressed fibres taken at different times varied from 1063 cm^{-1} to 1064.5 cm^{-1}. This is a significant variation, so the position of the peak of the free unstressed fibre was always measured and the peak shift relative to that value is quoted, not the absolute peak wavenumber.

4. Results and discussion

4.1. Regular single fibre pull-out test

Fig. 4 illustrates the stress–displacement curve for an ammonia plasma treated Spectra 900 fibre in an epoxy matrix cured at a temperature of 100 °C. The free fibre length was 10 mm, the constant rate of displacement was 1 mm min^{-1} and the embedded length l_e was 5 mm. Similar curves were obtained for all values of $l_e \geq 2$ mm. Most of the interesting features occur in this curve before the displacement reaches 1 mm, so the main plot is an expanded view of this part. The inset shows the whole curve. Initially the fibre is perfectly bonded to the epoxy matrix and the stress increases linearly with fibre displacement. The compliance of the free fibre is much greater than that of the composite, so this part of the curve relates to the elastic deformation of the free fibre. There is a stress drop at the point marked "Debonding", and at this load interfacial debonding starts at the point where the fibre enters the matrix. The stress drop can be detected when the free fibre length is small. Debonding from the matrix increases the compliance, as it increases the fibre length that is largely free (apart from the effects of friction). If the original free fibre is too long the effect will be too small to detect.

From then until the point marked "Pull-out" the debonding propagates along the fibre as the stress rises again, more slowly. The stress is increasing by a small amount because the extra stress is only required to overcome friction, to apply the stress required for debonding to a further part of the fibre. At the same time the compliance of the system is increasing as more of the fibre is weakly connected to the matrix. The pull-out process was monitored using a polarizing optical microscope. Fig. 5 shows a photomicrograph taken without polarizers and the same region taken with polarizers crossed at 0 and 90° to the fibre direction. The fibre is the same as that used in Fig. 4 and the micrographs were taken when the fibre was at the partially debonded stage, between the points marked "Debonding" and "Pull-out" in that figure. In the debonded part of the composite, the interface appears in strong contrast as a dark line in the photomicrograph taken without polarizers. In the bonded region the interface is visible only with difficulty. We can see the propagation of the fibre debonding as the dark lines on either side of the fibre extend. This can be related directly to the stress–displacement curve. The bright region around the fibre at the debonding front in the micrograph taken with crossed polarizers shows where the matrix is birefringent due to stress. It is most distinct when the orientation of the polarized light is at 0 or 90° to the fibre axis. This shows that the molecular extension or compression is at $\pm 45°$, due to a shear stress concentration near the debonding front.

At the point in Fig. 4 marked "Pull-out" there is a large stress drop. The peak stress at this point is the fibre pull-out stress, σ_p (Equation 1). Here the debonding is complete, and the fibre suddenly slips through the matrix until a new equilibrium is reached

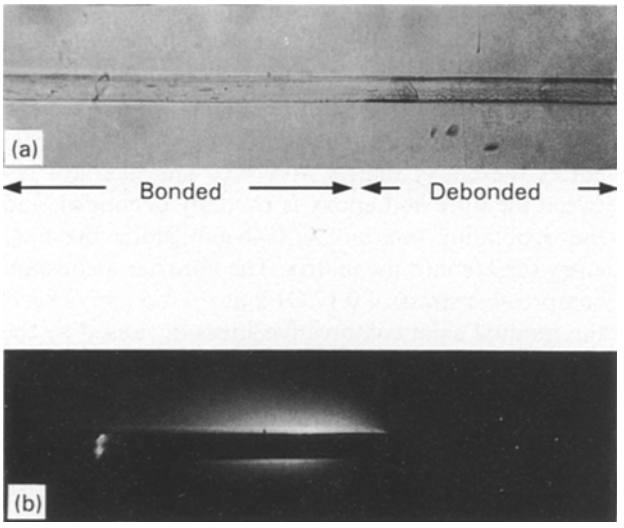

Figure 5 Photomicrographs of a partially debonded fibre. The fibre is pulled from the right and debonding propagates from right to left. (a) Unpolarized light; the debonded part of the interface appears as a dark line. (b) Polarized light; the same region with polarizers crossed at 0 and 90° to the fibre axis. The light region is where there are significant shear stresses in the matrix.

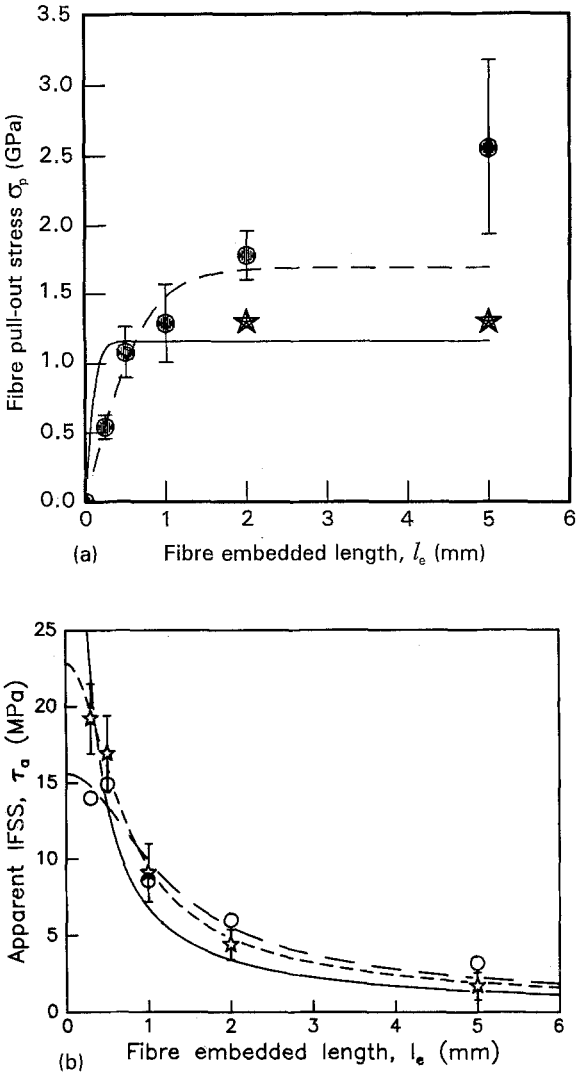

Figure 6 Fibre pull-out stress σ_p and apparent interfacial shear stress (IFSS), τ_a as a function of fibre embedded length l_e. (○) raw data (☆) corrected for friction (——) fit through all raw data (– – –) fit through corrected data (——) fit through corrected data, assuming static stress transfer length.

where the stress is lower and the resistance to fibre motion is due to friction. Pull-out then continues against the resistance of interfacial friction, until the whole embedded length is pulled out of the matrix. If the free fibre length is large, this part of the curve can show wide variations, from immediate complete pull-out to large stick-slip type oscillations of load [47]. These are due to the interaction of the stored elastic energy of the free fibre and the frictional resistance of the matrix, and are best avoided by using small free fibre lengths. Once all the fibre is debonded, there is no region of birefringence to be seen.

Fig. 6 shows the experimental fibre pull-out stress σ_p and the average or apparent interfacial shear strength, τ_a, derived from Equation 1 as a function of embedded length, l_e. It can be seen that σ_p increases continuously with l_e. The increase is proportional to embedded length at 0.25 and 0.5 mm, and the slope then falls. According to Equation 1, τ_a is approximately the same for both the two smallest lengths, and then falls. When the embedded length is less than 1 mm, the fibre is fully pulled out catastrophically upon initiation of interfacial debonding. This should happen at some small value of l_e, since the free fibre length is kept constant. In proportion to the embedded length, the free fibre length is becoming larger and elastic energy stored in the free fibre will dominate the pull-out process. When the embedded length is larger than 1 mm, the fibre pull-out proceeds as described above by a stable propagation of the debonding along the interface. The effect of friction may therefore become increasingly important at lengths over 1 mm. The measured pull-out stress σ_p is the stress for initiation of debonding plus the stress required for propagation of the debonding. The fibre pull-out stress increases much more slowly during this propagation step (Fig. 4) so σ_p increases slowly with l_e and τ_a, and averaged over the embedded length, becomes smaller. The stresses indicated as solid stars are estimates of the pull-out stress when the effects of friction are removed (this is σ_d). Open stars in the lower part of the figure are values of τ_a from pull-out stresses corrected for friction and for residual stress. These corrected data and the curves fitted to the data use the results from Raman spectroscopy and will be discussed in the following section.

4.2. Raman spectroscopy applied to fibre pull-out

Fig. 7 shows the Raman spectra of a free single fibre, of the pure epoxy and of a single fibre embedded in the center of a 1 mm thick block of epoxy. The three peaks at 1064, 1135, and 1295 cm^{-1} from the free fibre correspond to the C–C asymmetric and symmetric stretching modes, and the C–H twisting mode, respectively. The C–C symmetric stretch band in the fibre is

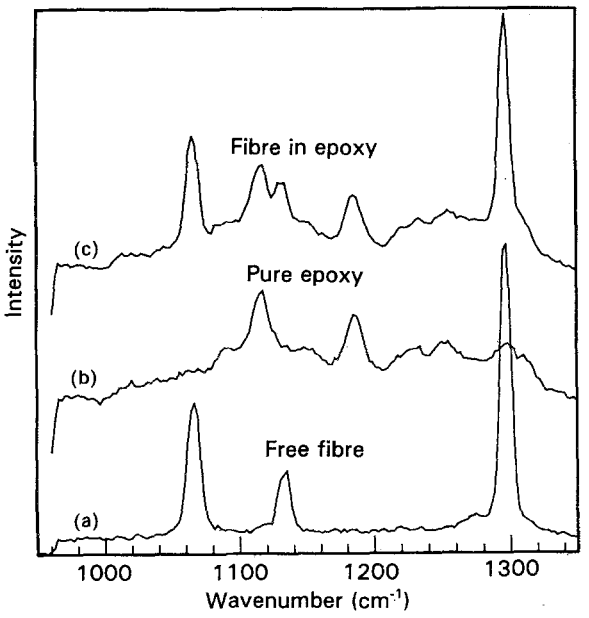

Figure 7 Raman spectra of (a) a free fibre, (b) pure epoxy, and (c) a fibre embedded in epoxy. The curves are shifted vertically for clarity.

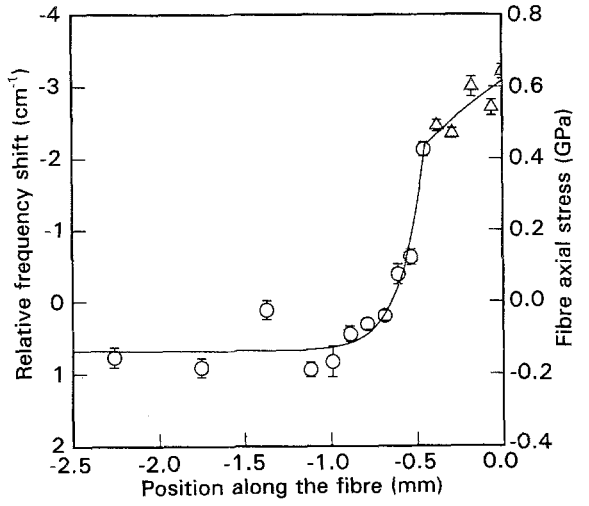

Figure 8 Wavenumber shift of the C–C asymmetric stretch band and derived fibre axial stress as a function of position along the fibre. The fibre is an ammonia plasma treated Spectra 1000 fibre which is partially debonded from the epoxy matrix (△) debonded; (○) bonded.

weaker than the C–C asymmetric stretch bands; it was stronger in previous studies [15] using a very similar system. It can be seen from Fig. 7 that only the C–C asymmetric stretch band is well separated from the bands of the epoxy spectrum. The other Raman bands in the polyethylene spectrum interfere or superimpose with bands of the epoxy spectrum. The C–C asymmetric stretch bands were fitted with a Gaussian–Lorentzian sum function and a quadratic background to exclude the slight interference of the epoxy background.

Fig. 8 shows the shift of the C–C asymmetric stretch bands in wavenumbers and on the right hand vertical axis the fibre axial stress derived from these shifts. The negative shift value represents the fibre in tension while the positive shift value represents the fibre in compression. The horizontal axis is the position along the fibre, which was an ammonia plasma treated Spectra 1000 fibre held under a fixed strain. The fibre enters the epoxy matrix at $x = 0$. The interface between the fibre and epoxy is partially debonded, and the debonding interface is 0.46 mm along the fibre entry surface into the matrix. The fibre has a constant compressive stress of 0.17 GPa at $l > 1.5$ mm. This is the residual axial compressive stress σ_r caused by the difference in axial TCE of the fibre and matrix. Along the debonded part of the fibre the relative frequency shift changes slowly at about 2 $cm^{-1}\,mm^{-1}$. This corresponds to an interfacial shear stress of approximately 2.8 MPa. The data for this debonded part of the fibre has been fitted with the expression derived for frictional resistance (Equation 37). However, there are too few data points to produce reliable information about the normal stress and frictional coefficient from this plot. The stress drops much more quickly from the debonding front along the bonded interface. The data for this bonded part of the fibre was fitted with the shear-lag theoretical expression for large l (Equation 31), since $l > 5/\beta$. A non-linear least square fitting program was used. The fit is a good one, as shown in Fig. 8, and we obtain:

$$\beta = 7.4 \pm 2\,mm^{-1} \quad \sigma_r = -0.17 \pm 0.03\,GPa$$
$$2\tau_s/r_f = 4 \pm 1\,MPa\,\mu m^{-1}$$

Taking $r = 14\,\mu m$ gives $\tau_s = 28 \pm 8$ MPa, which is twice the average interfacial shear strength obtained from the direct pull-out test of an embedded length of less than 0.5 mm, as shown in Fig. 6. To mimic the averaging over $l_e = 0.3$ mm, we take a linear least squares fit of the relative frequency shift at positions from 0.46 mm, which is the debonding front, to 0.76 mm along the bonded part of the fibre. The slope is $9.5 \pm 2\,cm^{-1}\,mm^{-1}$ and the average interfacial shear strength is 13.3 ± 3 MPa. This is the same as that obtained by direct fibre pull-out tests at embedded length $l_e = 0.3$ mm. According to Equation 14 the interfacial shear stress profile along the fibre is the differential of the tensile stress. Differentiating the fitted curves in Fig. 8 gives the interfacial shear stress profile shown in Fig. 9. The shear stress concentration at the position of the debonding front is clearly visible in this figure. It can also be seen from Figs 8 and 9 that the effective stress transfer length, where the axial stress drops by 90%, is only 0.3 mm.

How does this Raman result compare to those obtained from the normal pull-out test, and can the two tests be combined? Unfortunately a direct comparison may not be meaningful, because of the different time scales involved. The pull-out stress is measured after 30 s in a normal test (Fig. 4), and after 3.10^4 s in the Raman experiment (Fig. 3). Both fibre and matrix are viscoelastic, and may creep, so that mechanical tests on such different time scales should not give the same results. The simplest procedure for the analysis of the apparent IFSS data shown in Fig. 6(b) is to fit all the

points to Equation 2, without any corrections. The result is shown as the dashed line in Figs 6(a) and (b), which gives $\beta = 1.3\ mm^{-1}$ and $\tau_s = 15$ MPa. Taking residual stresses into account, that is, using Equation 22 instead of Equation 1 to define the apparent IFSS, changes these results considerably. Adding the residual compressive stress determined by Raman spectroscopy, 0.17 GPa, to the pull-out stresses shown in Fig. 6(a) increases the derived IFSS from 15 GPa to 21 ± 3 GPa and increases β to $1.8\ mm^{-1}$.

The pull-out stress σ_p at $l_e > 1$ mm, is increasing as shown in Fig. 6(a) only because of friction, and Equation 2, being used to fit these results, does not take friction into account. To correct for the effects of friction, the data at $l_e > 1$ mm is fitted to Equation 42 using reasonable values of α and γ [26]. The fitted value of the debonding stress σ_d, which would be the pull-out stress in the absence of friction, is then used instead of the measured pull-out stress. Because there are so few data points this is little more than using the value of σ_p at $l_e = 1$ mm for all longer embedded lengths, and the procedure gives the data points marked as stars in Fig. 6(a). The stars in Fig. 6(b) are data corrected for both friction and residual stress. In Fig. 6(b) the fit to Equation 2 is improved, but the effect on the derived parameters is not so great, the IFSS becomes 23 ± 3 GPa and β increases to $2.4 \pm 0.2\ mm^{-1}$. This is because the friction correction changes data at large embedded lengths, while the residual stress correction is more important at small embedded lengths, see Table I.

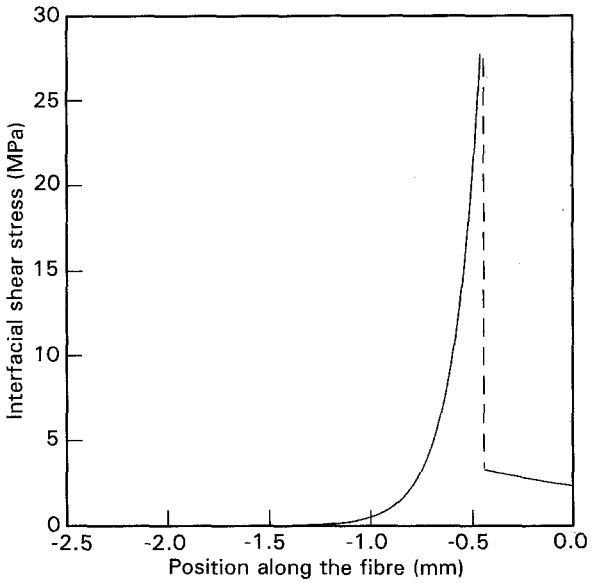

Figure 9 Interfacial shear stress profile obtained from the theoretical functions as shown in the previous figure, fitted to the experimental data.

TABLE I Original and corrected values of τ_a for different embedded lengths ℓ_e. τ_s is calculated by taking the Raman value of β

l_e (mm)	τ_a (MPa)	τ_a (MPa) corrected for residual stress	τ_a (MPa) corrected for friction	τ_s (MPa)
0.3	14	18.3	18.3	42
0.5	15	17.4	17.4	64
1.0	8	9	8.9	65
2.0	6	6.6	4.6	68
5.0	3.5	3.7	2.0	74

If we assume that the value of $\beta = 7.4\ mm^{-1}$ obtained from the semi-static Raman experiment is valid for the dynamic pull-out tests we can use Equation 2 to estimate τ_s from τ_a. The results are shown as the last column in Table I. The derived IFSS values are very high, higher than normally accepted for this system, and much higher than the bulk shear strength of the matrix. The fit to the pull-out test data with this value of β is shown in Fig. 6(b) as a solid line, and it is obviously not in good agreement with the data. This fitted curve gives a τ_s of 50 ± 5 MPa.

It was observed during the reloading process before the Raman spectrum was taken that interfacial debonding occurred at an external stress of 0.6 GPa. This is only half the debonding load during the regular pull-out tests, as shown in Fig. 6. Normal expectations are that slower experiments will give lower strengths and that creep will reduce local stress concentrations —in this case, that means an increase in the stress transfer length, smaller β. The analysis above shows that the IFSS is similar in the range of time scales investigated, but that β appears to be greater in the slower experiment. The shorter stress transfer length then results in a smaller pull-out load for the same IFSS. According to Equation 17 $\beta = \sqrt{2K/(E_f r_f)}$ where $K = G_m/r_f \ln(r_e/r_f)$ (Equation 13). In a linear elastic case, β depends on the ratio of matrix modulus to fibre modulus and will increase over time if the softening of the fibre exceeds that of the matrix. The shear-lag model which is the source of these expressions depends on the relative displacements of fibre

TABLE II β, τ_s and other parameters for a variety of composites

Reference	Composite system	β (mm^{-1})	τ_s (MPa)	E_f (GPa)	r_f (μm)	E_m (GPa)	K (GPa mm^{-1})	b_i μm	r_e/r_f
This study	Polyethylene/epoxy	7.4	57	70	14	1.5	28	20	4
This study	Polyethylene/epoxy	2.4	23	70	14	1.5	2.8	200	10^6
[9]	S-glass/phenolics	26.1	152	85	4.5	3	130	8.7	7
[9]	Graphite/polyimide	19.4	95	280	2.5	3	132	8	30
[7]	Graphite/epoxy	21.2	124	330	2.5	3	186	6.3	11
[7]	Graphite/epoxy	30.1	174	280	2.5	3	317	3.5	4

and matrix. When creep of the polyethylene fibre is involved it is the section of fibre under greatest axial load, at its entrance into the matrix, that will extend the most. This increased displacement will allow more stress transfer to the matrix, and so may reduce the stress transfer length and the pull-out load.

Other important parameters can be evaluated from the curve fitting where β is known. For $E_f = 70$ GPa [15] and $E_m = 1.5$ GPa, or $G_m = 0.56$ GPa [43] $\beta = 7.4\ mm^{-1}$, gives $K = 28\ GPa\ mm^{-1}$, $r_e/r_f = 4 \pm 0.5$, $b_i = 20\ \mu m$. Experimentally, the same results can be seen qualitatively from the birefringence pattern in Fig. 5. The region of birefringence in the epoxy extends only about one radius out from the fibre. As described in the analytical section above, if Equation 7 were correct, matrix shear would be inversely proportional to the radial distance from the fibre axis, so that $\tau(x, r_e)$ would be $\tau_i(x)/4$, and not negligible. To obtain this equation, Cox assumed that the matrix is deformed in pure shear, ignoring traction forces in the matrix due to Poisson's ratio differences between fibre and matrix. A correct elasticity analysis of the stress field [34] and finite element analysis [52] both show that the shear stress drops rather quickly in the matrix as one moves away from the fibre, decreasing more like r^{-2} than r^{-1}. Aside from these considerations, it is physically unreasonable that the specimen size should influence the interfacial shear stress when the specimen is large. Our result of $r_e/r_f = 4$ suggests that the effective radius r_e and not the sample outer dimension R should generally be used for evaluation of β. However, if the lower value of β obtained by fitting the corrected pull-out test data is used, very different results are obtained, with $b_i = 200\ \mu m$ and an even greater r_e, unrealistically large (Table II).

Table II compares β and τ_s obtained here using Raman spectroscopy with other published results. The other authors used regular single fibre pull-out tests and Equation 2 to obtain their results. In Fig. 10 β is plotted against τ_s and it can be seen that β is proportional to τ_s. The best fit straight line to the data gives $\beta = (0.18 \pm 0.01)\tau_s$. This is an entirely empirical result, and it seems unreasonable that the stress distribution should depend on the interfacial shear strength at low loads. Fan *et al.* [20] showed that the stress distribution in a poly(diacetylene) fibre/epoxy system remained the same when the fibre was coated with a silicone release agent to reduce the interfacial shear strength. Their results were obtained at low stresses, before interfacial failure; this would indicate that the empirical result given above relates only to β and τ_s obtained under failure conditions. Since it refers to a parameter from shear-lag theory, it is relevant to ask what would be the effects of this relation on the equations derived in the analytical section. One would be that the debonding stress, (the pull-out stress neglecting friction), σ_d, is approximately equal to $1/r_f + \sigma_r$. This indicates that for the range of samples considered, which were all well bonded initially, differences in pull-out strength relate more to the differences in fibre radius than to specific surface interactions. Thus comparisons between surface treatments should be made in systems with the same fibre radius.

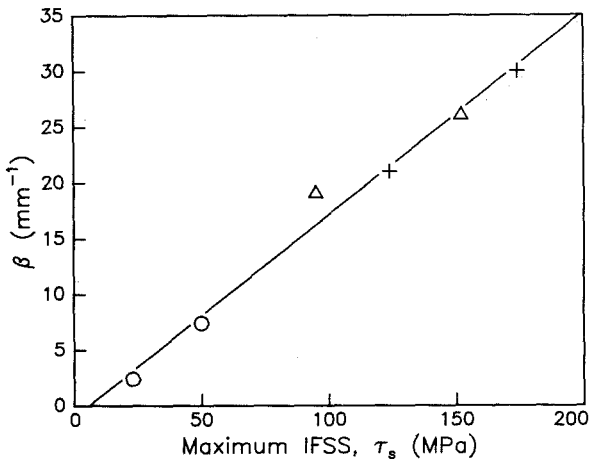

Figure 10 β as a function of the interfacial shear strength, τ_s, for a variety of fibre composite materials (○) this study; (△) Désarmot and Favre; (+) Pikethly and Doble.

For comparison, we can also calculate K, b_i and r'_e/r_f for other composite systems from the values given for β in Table II. Because the published information is incomplete, the fibre and matrix moduli E_f and E_m are taken as typical values from handbooks [53] and from manufacturer's data sheets. The results are shown in Table II. It can be seen that K is lowest for the polyethylene fibres studied here and highest for graphite fibres. b_i and r_e decrease as τ_s increases for graphite fibre composites. b_i is only a few times r_f while r_e, which is $r_f \exp(b_i/r_f)$ may be tens of times r_f. Shear birefringence in these composites gives an r_e tens of times r_f, and larger in lower modulus matrices [43, 54, 55]. The disagreement between theoretically predicted values of b_i and r_e and the experimental evidence suggests that neither of the shear-lag treatments of the interaction of the interface and the matrix [1, 2] is sufficient. It appears that values of r_e/r_f agree reasonably well with those obtained from matrix birefringence in the case of systems with lower τ_s, such as polyethylene/epoxy and graphite/polyimide. In the other systems τ_s is much larger than the yield stress of the matrix and this suggests that a purely elastic approach cannot be correct.

5. Conclusions

We have shown that measurement of polymer fibre stress distribution by Raman spectroscopy can be applied to the fibre pull-out test. This gives the quasi-static interfacial shear stress as a function of position along the fibre. The theoretical stress distribution derived from the interfacial shear-lag theory fits this experimental data well with a stress transfer length of 0.3 mm for a high modulus polyethylene fibre/epoxy model composite. The stress distribution during interfacial debonding allows the direct measurement of the maximum interfacial shear strength. A value of 28 MPa for IFSS is obtained from static measurement

of a debonding front, while the apparent average value obtained from the single fibre pull-out test is 24 MPa. The analysis of the pull-out tests gives a larger effective stress transfer length, 1 mm. If the static stress distribution obtained by Raman spectroscopy is taken to exist in the pull-out test, the derived IFSS is much larger, 50 ± 5 MPa. The actual stress distribution allows us to calculate other parameters of the system, such as the shear-lag constant K and the effective interfacial radius and thickness, r_e and b_i.

The smaller stress transfer length gives the effective interfacial thickness, b_i, as 20 μm using $K = G_m/b_i$ [2]. Observation of shear stress birefringence in the optical microscope is in qualitative agreement with this. The fibre diameter is 28 μm, so the interfacial shear stress transfer distance normal to the fibre axis is close to the fibre diameter. Using $K = G_m/r_e \ln(r_e/r_f)$ according to Cox [1], $r_e/r_f = 4$ from K. The larger stress transfer length which gives a more acceptable value for IFSS gives unreasonably large interfacial thicknesses. b_i and r_e obtained for other composites using shear-lag theory are also inconsistent with shear birefringence experiments when τ_s is much larger than the yield strength of the matrices. This shows that neither treatment of the interaction between the interface and matrix is satisfactory. Since both are entirely elastic, with no consideration of plastic or viscoelastic deformation at the interface, this should not be surprising. On comparing our values of β and τ_s with those for other composites, we find empirically that $\beta = (0.18 \pm 0.01)\tau_s$.

Acknowledgements

This work is supported by the Cornell University Material Science Center which is supported by the National Science Foundation, DMR. Mr J. Eun assisted with the Raman spectroscopy and Mr E. Hsu worked on the single fibre pull-out test. The authors would like to express their gratitude to Professor A. Rouff and Y. Vohra for access to the Raman spectrometer, and to Professor C. -Y. Hui for constructive discussions over the section on the analytical aspects and Professor P. Schwartz for reviewing this manuscript.

References

1. H.L.COX, *Brit. J. Appl. Phys.* **3** (1952) 72.
2. L. B. GRESZCZUK, in "Interfaces in composites", ASTM STP 452 (ASTM, Philadelphia, PA, USA, 1969) p. 42.
3. Z. GAO and K. L. REIFSNIDER, in Proceedings of the 6th Technical Conference of American Society for Composites, Albany, New York (Technomic, Lancaster, PA, USA, 1991) p. 742.
4. M. R. PIGGOT, *Mater. Res. Soc. Symp. Proc.* **170** (1990) 265.
5. A. GARTON, G. HALDANKAR and E. SHOCHEY, *ibid.* **170** (1990) 291.
6. A. N. NETRAVALI, Z. -F. LI, W. SACHSE and F. H. WU, *J. Mater. Sci.* **26** (1991) 6631.
7. M. J. PITKETHLY and J. B. DOBLE, *Composites* **21** (1990) 389.
8. B. MILLER, P. MURI and L. REBENFELD, *Composites Sci. Technol.* **28** (1987) 17.
9. G. DÉSARMOT and J. -P. FAVRE, *ibid.* **42** (1991) 151.
10. M. R. PIGGOT and Z. N. WANG, in Proceedings of the 6th Technical Conference of American Society for Composites, Albany, New York (Technomic, Lancaster, PA, USA, 1991) p. 725.
11. C. GALIOTIS, I. M. ROBINSON, P. N. BATCHELDER and R. J. YOUNG, in "Engineering applications of new composites", edited by S. A. Paipetis and G. C. Papanicolaou (Omega Scientific, Wallingford, UK, 1988).
12. R. J. DAY, I. M. ROBINSON, M. ZAKIKHANI and R. J. YOUNG, *Polymer* **28** (1987) 1833.
13. D. N. BATCHELDER and D. BLOOR, *J. Polym. Sci. Polym. Phys. Ed.* **17** (1979) 569.
14. R. J. YOUNG, R. J. DAY, M. ZAKIKHANI and I. M. ROBINSON, *Composites Sci. Technol.* **34** (1989) 243.
15. K. PRASAD and D. T. GRUBB, *J. Polym. Sci.* **B27** (1989) 381.
16. B. J. KIP, M. C. P. van EIJK and E. J. MEIER, *ibid.* **B29** (1991) 99.
17. D. T. GRUBB and Z. -F. LI, *Polymer* (1991) **33** (1992) 2587.
18. J. A. H. M. MOONEN, W. A. C. ROOVERS, R. J. MEIER and B. J. KIP (1992) *J. Polym. Sci. B, Polym. Phys.* **30** (1992) 361.
19. C. GALIOTIS, R. J. YOUNG, P. H. YEUNG and D. N. BATCHELDER, *J. Mater. Sci.* **19** (1984) 3640.
20. C. F. FAN, D. A. WALDMAN and S. L. HSU, *J. Polym. Sci. B Polym. Phys.* **29** (1991) 235.
21. H. JAHANKHANI and C. GALIOTIS, in "Interfaces in polymer, ceramic and metal matrix composites", edited by H. Ishida (Elsevier Science, New York, USA, 1988) p. 107.
22. C. GALIOTIS, *Composites Sci. Technol.* **42** (1991) 125.
23. N. MELANTIS and C. GALIOTIS, *J. Mater. Sci.* **25** (1990) 5081.
24. D. T. GRUBB and Z. -F. LI, IUPAC 33rd Symposium on Polymers, Session 2.1.2 Book of Abstracts (IUPAC, Montreal, 1990).
25. L. C. N. BOOGH, R. J. MEIER, H. -H. KAUSCH and B. J. KIP, *J. Polym. Sci. B Polym. Phys.* **30** (1992) 325.
26. D. T. GRUBB and Z. -F. LI, *J. Mater. Sci.* (1993) submitted.
27. N. S. MURTHY, S. T. CORREALE and S. KAVESH, *Polym. Commun.* **31** (1990) 50.
28. P. LAWRENCE, *J. Mater. Sci.* **7** (1971) 1.
29. J. AVESTON and A. KELLY, *ibid.* **8** (1973) 352.
30. P. S. CHUA and M. R. PIGGOT, *Composites Sci. Technol.* **22** (1985) 33.
31. B. BUDIANSKY, J. W. HUTCHINSON and A. G. EVANS, *J. Mech. Phys. Solids* **34** (1986) 167.
32. R. MUKI and E. STERNBERG, *Int. J. Solids Structures* **6** (1970) 69.
33. E. F. FORD, Technical Report No. 1, NSF Grant GH-33576, Division of Applied Sciences, Harvard University (1973).
34. L. N. McCARTNEY, *Proc. R. Soc. Lond. A* **425** (1989) 215.
35. P. S. STEIF and S. F. HOYSAN, *Mech. Materials* **5** (1986) 375.
36. L. S. SIGL and A. G. EVANS, *ibid* **8** (1989) 1.
37. J. W. HUTCHINSON and H. M. JENSEN, *ibid.* **9** (1990) 139.
38. W. B. TSAI and T. MURA, in Proceedings of the 6th Technical Conference of American Society for Composites, Albany, New York, (Technomic, Lancaster, PA, USA, 1991) p. 538.
39. R. J. GRAY, *J. Mater. Sci.* **19** (1984) 861.
40. F. J. McGARRY and M. FUJIWARA, in Proceedings of the 23rd Annual Technical Conference, Reinforced Plastic Composites Division (The Society of Plastics Industry, Inc., New York, 1968).
41. B. AKSEL, C. -Y. HUI and D. C. LAGOUDAS, *Int. J. Solids Structures* **27** (1991) 833.
42. Z. M. ASLOUN, M. NARDIN and J. SCHULTZ, *J. Mater. Sci.* **24** (1989) 1835.
43. A. N. NETRAVALI, R. B. HENSTENBURG, S. L. PHOENIX and P. SCHWARTZ, *Polym. Composites* **10** (1989) 226.
44. S. TIMOSHENKO, "Strength of materials" (MacMillan, London, UK, 1941).
45. D. J. PINCHIN and D. TABOR, *J. Mater. Sci.* **13** (1978) 1261.
46. M. R. PIGGOT, *Composites Sci. Technol.* **30** (1987) 295.
47. Z. -F. LI, A. N. NETRAVALI and W. SACHSE, *J. Mater. Sci.* (1992) **27** (1992) 4625.

48. Z. -F. LI and A. N. NETRAVALI, *J. Appl. Polym. Sci.* **44** (1992) 333.
49. U. GUAR and B. MILLER, in "Controlled interface in composite materials", edited by H. Ishida (Elsevier Science, New York, USA, 1991) p. 723.
50. R. A. HAAKSMA and M. CEHELNIK, *Mat. Res. Soc. Symp. Proc.* **170** (1990) 71.
51. P. SCHWARTZ, A. N. NETRAVALI and L. S. SEMBACK, *Textile Res. J.* **56** (1986) 502.
52. A. S. CARRARA and F. J. McGARRY, *J. Composite Mater.* **2** (1968) 22.
53. G. LUBIN, "Handbook of composites" (Van Nostrand Reinhold Co., New York, USA, 1982).
54. A. N. NETRAVALI, P. SCHWARTZ and S. L. PHOENIX, *Polym. Composites* **10** (1989) 385.
55. L. T. DRZAL, M. J. RICH and P. F. LLOYD, *J. Adhesion* **1** (1982) 16.

Received 10 April 1992
and accepted 4 January 1993